



# Investigation of the potential of using TiO<sub>2</sub> nanoparticles as a contrast agent in computed tomography and magnetic resonance imaging

Akasaka, Hiroaki ; Mukumoto, Naritoshi ; Nakayama, Masao ; Wang, Tianyuan ; Yada, Ryuichi ; Shimizu, Yasuyuki ; Inubushi, Sachiko ;...

---

**(Citation)**

Applied Nanoscience, 10(8):3143-3148

**(Issue Date)**

2020-08

**(Resource Type)**

journal article

**(Version)**

Accepted Manuscript

**(Rights)**

© King Abdulaziz City for Science and Technology 2019. This is a post-peer-review, pre-copyedit version of an article published in Applied Nanoscience. The final authenticated version is available online at: <https://doi.org/10.1007/s13204-019-01098-y>

**(URL)**

<https://hdl.handle.net/20.500.14094/90007446>



1 **Investigation of the potential of using TiO<sub>2</sub> nanoparticles as a contrast agent in computed tomography and**  
2 **magnetic resonance imaging**

3 Hiroaki Akasaka<sup>a</sup> \*, Naritoshi Mukumoto<sup>a</sup>, Masao Nakayama<sup>b</sup>, Tianyuan Wang<sup>c</sup>, Ryuichi Yada<sup>c</sup>, Yasuyuki  
4 Shimizu<sup>c</sup>, Sachiko Inubushi<sup>c</sup>, Katsusuke Kyotani<sup>d</sup>, Keisuke Okumura<sup>d</sup>, Masanori Miyamoto<sup>d</sup>, Ai Nakaoka<sup>c</sup>,  
5 Kenta Morita<sup>c</sup>, Yuya Nishimura<sup>c</sup>, Chiaki Ogino<sup>e</sup> and Ryohei Sasaki<sup>a</sup>

6

7 <sup>a</sup>Division of Radiation Oncology, Kobe University Hospital, Chuo-ku Kobe, Hyogo 650-0017, Japan

8 <sup>b</sup>Division of Medical Radiations School Health & Biomedical Sciences, RMIT University, Plenty Road,  
9 Bundoora, Victoria 3083, Australia

10 <sup>c</sup>Division of Radiation Oncology, Kobe University Graduate School of Medicine, Chuo-ku Kobe, Hyogo 650-  
11 0017, Japan

12 <sup>d</sup>Center for Radiology and Radiation Oncology, Kobe University Hospital, Chuo-ku Kobe, Hyogo 650-0017,  
13 Japan

14 <sup>e</sup>Department of Chemical Science and Engineering, Graduate School of Engineering, Kobe University, 1-1  
15 Rokkoudaicho, Nada-ku, Kobe, Hyogo 657-8501, Japan

16

17 \*Correspondence to: Hiroaki Akasaka, Division of Radiation Oncology, Kobe University Hospital, Chuo-ku  
18 Kobe, Hyogo 650-0017, Japan.

19 Tel: +81-78-382-5687; Fax: +81-78-382-6734.

20 E-mail: akasaka@harbor.kobe-u.ac.jp (H. Akasaka)

21

22 Keywords: Nanoparticle, Radiotherapy, Radiation diagnosis, Theranostic drug, titanium dioxide nanoparticles

23

---

24 **ABSTRACT**

25 Nanoparticles (NPs) are useful for radiotherapy. Currently, efforts are underway globally for the development of  
26 novel titanium dioxide NPs (TiO<sub>2</sub>-NPs) that exhibit both contrast effects and anti-tumor effects. In this study, the  
27 image contrast properties of TiO<sub>2</sub>-NPs were evaluated using a clinical magnetic resonance imaging (MRI)  
28 system and a clinical computed tomography (CT) scanner, as the use of TiO<sub>2</sub>-NPs as an anti-cancer agent has  
29 been reported in several reports. An obvious difference in visualization was observed between the control and  
30 TiO<sub>2</sub>-NP samples on T<sub>2</sub>-weighted images. These results suggest that TiO<sub>2</sub> can potentially be used as a novel  
31 theranostic drug with radiosensitizing ability and radiological diagnostic ability, through modification of  
32 chemical groups on its surface, and as a component of drug delivery systems.

33 Keywords: Nanoparticle, Titanium oxide, Theranostic, MRI, CT, Radiotherapy

34 **Background**

35 Radiation therapy is one of the major treatment modalities for cancer, in which ionizing radiation is  
36 used to kill cancer cells (Akasaka et al. 2016). An increased radiation dose would result in more effective  
37 elimination of the cancerous tissue. However, in some cases, the radiation dose cannot be increased due to the  
38 possibility of damage to nearby functional and healthy tissues, and this limits the efficacy of the treatment  
39 (Bump et al. 2003; Akasaka et al. 2014; T. Ruba et al. 2018); consequently, currently only a few effective  
40 radiotherapy techniques are available, and novel strategies need to be explored (Akasaka et al. 2014). Recently,  
41 there has been a rapid increase in the use of nanoparticles (NPs) for biological applications, and there is potential  
42 for their use in the diagnosis and treatment of human cancer (Yezhelyev et al. 2006; Kim et al. 2010; Service  
43 2005).

44 NPs have been extensively studied for their potential applications in the scientific field due to their  
45 unique electrical, magnetic, and visibility and their versatile functionality. Biomedical applications of NPs have  
46 attracted considerable attention because NPs are expected to improve medical diagnosis and treatment. Moreover,  
47 various NPs have been used as contrast agents in magnetic resonance imaging (MRI) and computed tomography  
48 (CT). Currently, the NPs under development for clinical imaging include gold NPs for X-ray contrast (Hainfeld  
49 et al. 2006), magnetic NPs for MRI enhancement (Fang and M. Zhang 2009), and also hybrid NPs containing  
50 iron oxide and gold in polymer coating, which can serve as contrast agents for both CT and MRI (Kim et al.  
51 2011).

52 In addition to their potential applications in imaging, NPs are also being investigated for their potential  
53 application in cancer therapy (Chatterjee et al. 2008; Wilson and Patterson 2008; Garnica-Garza 2009). They  
54 offer similar advantages over other contrast agents in this area as in imaging. In addition, it is also possible to  
55 design NPs that can selectively accumulate in cancer cells, thereby providing targeted treatment that may not be  
56 possible with conventional techniques (Chatterjee et al. 2008).

57 Several NPs made from titanium dioxide (TiO<sub>2</sub>-NPs) have been investigated worldwide for their  
58 potential application in cancer therapy. Some studies have shown that irradiation of TiO<sub>2</sub>-NPs generates free-  
59 radicals that facilitate the spontaneous generation of reactive oxygen species (ROS) (Jin et al. 2011; Townley et  
60 al. 2012; Yin et al. 2012; Babaei and Ganjalikhani 2014). In vivo studies using TiO<sub>2</sub>-NPs have demonstrated a  
61 significant decrease in tumor volume when these NPs are irradiated with 200-kV X-rays (Nakayama et al. 2016).  
62 Moreover, recent in vitro studies on glioma cells have demonstrated the potential use of such NPs for  
63 photodynamic therapy (Yamaguchi et al. 2010). Ultrasonic stimulation of TiO<sub>2</sub>-NPs has been shown to kill NP-  
64 impregnated glioma cells in a manner similar to that of ultraviolet stimulation of TiO<sub>2</sub>-NPs (Allison et al. 2010).  
65 Other studies have shown that TiO<sub>2</sub>-NPs are also essentially non-toxic (Bischoff and Bryson 1982; Bernard et al.  
66 1990; Fabian et al. 2008) and hence hold considerable promise as cancer therapy agents.

67 Currently, the development of novel TiO<sub>2</sub>-NPs with both the potential to be used as a contrast agent and  
68 as well as to produce anti-tumor effects is under investigation all over the world. Although several studies have  
69 investigated the imaging properties of TiO<sub>2</sub>-NPs, they have all used TiO<sub>2</sub>-NPs that have been chemically  
70 modified. To our knowledge, the imaging properties of unmodified TiO<sub>2</sub>-NPs have not been investigated thus far.  
71 Hence, in this study, we investigated the visibility of TiO<sub>2</sub>-NPs using clinical MRI and CT scanning in an  
72 attempt to determine their image contrast properties.

## 73 **2. Materials and methods**

74

### 75 *2.1. Transmission electron microscopy and dynamic light scattering of nanoparticle "TiO<sub>2</sub>"*

76 The TiO<sub>2</sub>-NPs used in this study were purchased from Ishihara Sangyo, Ltd. (Osaka, Japan). The size  
77 and morphology of the TiO<sub>2</sub>-NPs were evaluated using a transmission electron microscope (TEM) (JEM-  
78 1200EX, JEOL Ltd., Tokyo, Japan) as described previously (Srivastava et al. 2013). The TEM images were  
79 obtained at an acceleration voltage of 80 kV. Dynamic light scattering (DLS) was performed using a Malvern

80 Zetasizer ZS (Malvern Panalytical Ltd, Malvern, United Kingdom) to estimate the hydrodynamic diameter of the  
81 TiO<sub>2</sub>-NPs.

## 82 *2.2. Magnetization measurement*

83 The variation in the magnetic moment was carried out by altering the applied field from 10,000 Oe to  
84 10,000 Oe at 25.2°C. This measurement was performed by Toei Industry Co., Ltd. (Tokyo, Japan). To correct  
85 for the diamagnetic contribution of the sample tube, the magnetic moment of the empty sample tube and sample  
86 holder was subtracted from the data sets; however, due to the high magnetization values obtained from the NP  
87 sample, the contribution of the sample tube and holder was considered negligible and was ignored.

## 88 *2.3. Cell culture and viability assessment*

89 MIAPaCa-2 cells were obtained from the American Type Culture Collection (Manassas, VA, USA) and  
90 cultured in Roswell Park Memorial Institute 1640 medium supplemented with 10% fetal bovine serum, penicillin  
91 (100 U/mL), and streptomycin (100 µg/mL). The anti-tumor effect, in combination with the radiation treatment,  
92 was assessed with the colony forming assay. For the colony forming assay, MIAPaCa-2 cells were treated with  
93 0.1 mg/mL TiO<sub>2</sub>-NPs or saline for 1 h, and then exposed to 0, 2, 4 and 8 Gy of radiation. After 9–12 days,  
94 colonies were fixed with a solution of 10% methanol and 20% acetic acid, stained with methylene blue, and  
95 counted under a light microscope.

## 96 *2.4. X-ray irradiation*

97 X-ray irradiation was performed using an MBR-1505R2 instrument (Hitachi, Tokyo, Japan) at a voltage  
98 of 150 kV and a current of 5 mA with a 1-mm-thick aluminum filter (0.5 Gy/min at the target) for in vitro  
99 studies.

## 100 *2.5. CT imaging*

101 CT images were acquired using Aquilion LB (TOSHIBA Medical Systems, Tochigi, Japan). Imaging  
102 parameters were as follows: slice thickness, 1.0 mm; tube energy, 120 kVp, 300 mA; field of view (FOV), 320  
103 mm; matrix, 512 × 512. CT data were analyzed using the Hounsfield units (HU) for regions of interest. The  
104 concentrations of the TiO<sub>2</sub>-NPs used are shown in Table 1.

## 105 *2.6. MR imaging*

106 MR imaging experiments were performed on a 3.0 T MR unit (Ingenia, PHILIPS, Amsterdam,  
107 Netherlands). Two pulse sequences were used. One was a T<sub>1</sub>-weighted SE-XL/90 sequence with the following  
108 parameters: relaxation time (TR) = 4000 ms; echo time (TE) = 16 ms; FOV = 260 mm; matrix = 512 × 512; and  
109 slice thickness = 3 mm. the other was a T<sub>2</sub>-weighted FSE-XL/90 sequence with the following parameters: TR =  
110 4000 ms; TE = 100 ms; FOV = 260 cm; matrix = 512 × 512; slice thickness = 3 mm. The concentrations of the  
111 TiO<sub>2</sub>-NPs used are shown in Table 1.

## 112 *2.7. Statistical analysis*

113 Data are presented as mean ± standard error. Differences between groups were evaluated with the  
114 Student's t test. Data were considered statistically significant at P < 0.05.

## 115 **3. Results**

### 116 *3.1. TEM and DLS*

117 Considering enhanced permeability and retention effects of TiO<sub>2</sub>-NPs, we aimed to prepare NPs with a size  
118 of less than 100 nm (Maeda et al. 2000; Perrault et al. 2009; Huo et al. 2013). The diameter of the TiO<sub>2</sub>-NPs was  
119 determined to be approximately 50 nm using TEM (Fig. 1a). Consistent with the TEM images, the diameter of  
120 the TiO<sub>2</sub>-NPs was determined to be approximately 50-100 nm using DLS, with a narrow unimodal size  
121 distribution (Fig. 1b).

### 122 *3.2. Magnetic properties*

123 Fig. 2 shows the magnetization of TiO<sub>2</sub>-NPs at 25.2°C. The saturation magnetization (M<sub>s</sub>) value for  
124 TiO<sub>2</sub>-NPs was 9.711 × 10<sup>-4</sup> emu and the remanence (M<sub>r</sub>) was 4.269 × 10<sup>-6</sup> emu. The TiO<sub>2</sub>-NPs showed weak  
125 diamagnetic behavior.

### 126 *3.3. Cell viability assessment*

127 The colony forming assay results revealed fewer MIAPaCa-2 cell colonies on treatment with the  
128 combination as compared to irradiation alone (\*P < 0.05 and \*\*P < 0.1) (Fig. 3).

### 129 *3.4. CT imaging and MR imaging*

130 The CT numbers for the control group and for the different concentrations of TiO<sub>2</sub>-NPs used are shown  
131 in Fig. 4(a) and Table 1. Contrast-enhanced CT images are shown in Fig. 4(b). The uncertainty in each

132 measurement (represented by the standard deviation of the Hounsfield unit measurement) was 0.3 HU. The  
133 sensitivity of the TiO<sub>2</sub>-NPs to detection with MRI was determined. The T<sub>1</sub> and T<sub>2</sub> values for the control group  
134 and for the different concentrations of TiO<sub>2</sub>-NPs used are shown in Fig. 4(c, e) and Table 1. Contrast-enhanced  
135 T1W and T2W images are shown in Fig. 4(d, f) and Table 1.

#### 136 **4. Discussion**

137 NPs are being studied all over the world, and have the potential to be used as novel therapeutic agents  
138 for cancer. In particular, TiO<sub>2</sub>-NPs have great potential for this application. For example, they can be used as  
139 anti-tumor agents by incorporating them in drug delivery systems. Therefore, in this study, we investigated the  
140 visibility of TiO<sub>2</sub>-NPs using clinical MRI and CT scanning in an attempt to determine their image contrast  
141 properties.

142 No obvious aggregation was observed in the representative TEM image of the NPs depicted in Fig. 1a.  
143 Fig. 1b shows the size distribution of the NPs. The diameter was about 50–100 nm, which is suitable for the  
144 enhanced permeability and retention effects.

145 Leon Smith et al. indicated the CT value of their TiO<sub>2</sub>-NPs in their publication and concluded that a  
146 TiO<sub>2</sub>-NP concentration of greater than 15 mg/mL produced detectable changes in the CT number (Leon et al.,  
147 2012). In our study, the maximum concentration used was 5.0 mg/mL. Because of the low concentration of  
148 TiO<sub>2</sub>-NPs, there was no difference in the imaging properties between the TiO<sub>2</sub>-NPs and the control sample in our  
149 CT measurements; a gradual increase in CT value was observed in the investigated concentration range. In  
150 general, the atomic number of water is nearly 7, and that of the bone is nearly 20 because bone is composed  
151 almost entirely of calcium. In this study, the visualization in TiO<sub>2</sub>-NPs and control samples was almost the same  
152 because of the low concentration of TiO<sub>2</sub>-NPs. Hence, for TiO<sub>2</sub>-NPs to be used for enhancement in MRI, their  
153 concentration in the tumor needs to be increased.

154 As shown in Fig. 2, TiO<sub>2</sub>-NPs exhibited paramagnetic properties. This property is same as that of the  
155 small particulate gadolinium oxide (SPGO) enhancement agent (Gholamreza et al., 2012). Our results indicated  
156 that these findings regarding TiO<sub>2</sub>-NPs are in line with the findings of previous research.

157 In magnetization measurements, TiO<sub>2</sub>-NPs were observed to be weakly diamagnetic. On MRI, the  
158 imaging properties showed no difference between control and TiO<sub>2</sub>-NPs on T<sub>1</sub>-weighted imaging. However, the  
159 sensitivity to detection by MRI improved at higher concentrations of TiO<sub>2</sub>-NPs, and there was a significant

160 difference in the  $T_2$  value between control and  $\text{TiO}_2$ -NP samples at higher concentrations of  $\text{TiO}_2$ -NPs. These  
161 results show that  $\text{TiO}_2$ -NPs offer great potential for use in  $T_2$ -weighted MRI. As shown in Fig. 4(f),  $T_2$ -weighted  
162 images change drastically in signal intensity with an increasing  $\text{TiO}_2$ -NP concentration, indicating that  $\text{TiO}_2$ -NPs  
163 generated MRI contrasts on transverse ( $T_2$ ) proton relaxation time-weighted sequences. Fig. 4(e) shows the  
164 relaxation rate  $1/T_2$  as a function of  $\text{TiO}_2$  concentration in  $\text{TiO}_2$ -NPs. The relaxation rates varied linearly with the  
165 titanium concentration, according to the following equation:

$$166 \quad 1/T_2 = 1/T_2^0 + r_2[\text{TiO}_2]$$

167 where  $1/T_2$  is the observed relaxation rate in the presence of  $\text{TiO}_2$ -NPs,  $1/T_2^0$  is the relaxation rate of pure water,  
168  $[\text{TiO}_2]$  is the concentration of  $\text{TiO}_2$ -NPs, and  $r_2$  is the transverse relaxivity, which represents the efficiency of  
169  $\text{TiO}_2$ -NPs, as a contrast agent shortens the proton relaxation times. The  $r_2$  value of  $\text{TiO}_2$ -NPs was  $5 \times 10^{-4}$   
170  $\text{mg/mL}^{-1}\text{s}^{-1}$ . In addition, Fig. 4(c) shows the relaxation rate  $1/T_1$  as a function of  $\text{TiO}_2$  concentration in  $\text{TiO}_2$ -NPs.  
171 The relaxation rates were stable with the titanium concentration, according to the following equation:

$$172 \quad 1/T_1 = 1/T_1^0 + r_1[\text{TiO}_2]$$

173 where  $1/T_1$  is the observed relaxation rate in the presence of  $\text{TiO}_2$ -NPs,  $1/T_1^0$  is the relaxation rate of pure water,  
174  $[\text{TiO}_2]$  is the concentration of  $\text{TiO}_2$ -NPs, and  $r_1$  is the longitudinal relaxivity, which represents the efficiency of  
175  $\text{TiO}_2$ -NPs, as a contrast agent shortens the proton relaxation times. The  $r_1$  value of  $\text{TiO}_2$ -NPs was  $1 \times 10^{-5}$   
176  $\text{mg/mL}^{-1}\text{s}^{-1}$ , suggesting that  $\text{TiO}_2$ -NPs are superior as a  $T_2$ -shortening agent than as a  $T_1$ -shortening agent.  
177 **Additionally,  $\text{TiO}_2$ -NPs exhibit anti-tumor effect when combined with radiation, as shown in Fig.3. The result of**  
178 **the colony-forming assay indicated the radiosensitizing potential of  $\text{TiO}_2$ -NPs similar to that of the reported**  
179 **novel radiosensitizer, titanium peroxide NPs ( $\text{TiOx}$ -NPs) (Nakayama at al. 2016).**

## 180 **5. Conclusions**

181 In summary,  $\text{TiO}_2$ -NPs offer considerable promise for use as contrast agents in MRI, especially  $T_2$ -  
182 weighted MRI. **Our previous study showed that  $\text{TiOx}$ -NPs have anti-tumor effect (Nakayama at al. 2016). In this**  
183 **study, we observed that  $\text{TiO}_2$ -NPs that is used for preparing titanium peroxide also have anti-tumor effects.**  
184 **Additionally, the results show that titanium dioxide also exhibits imaging visibility.** Thus, they have the potential  
185 to be used as novel theranostic drugs with radiosensitizing and radiological diagnostic abilities via modification  
186 of the chemical groups on their surface and use in conjunction with drug delivery systems. The findings of the  
187 present study indicate that using  $\text{TiO}_2$ -NPs can be an effective strategy for radiation treatment and cancer



188 diagnosis. Future clinical applications of those NPs require rigorous surface engineering and careful toxicity  
189 evaluation.

190

191 **References**

- 192 Akasaka H, Mizushina Y, Yoshida K, Ejima Y, Mukumoto N, Wang T, Inubushi S, Nakayama M, Wakahara Y,  
193 Sasaki R (2016) MGDG extracted from spinach enhances the cytotoxicity of radiation in pancreatic cancer cells.  
194 *Radiat Oncol* 11(1):153
- 195 Akasaka H, Sasaki R, Miyawaki D, Mukumoto N, Sulaiman NS, Nagata M, Yamada S, Murakami M, Demizu Y,  
196 Fukumoto T (2014) Preclinical evaluation of bioabsorbable polyglycolic acid spacer for particle therapy. *Int J*  
197 *Radiat Oncol Biol Phys* 90(5):1177–1785. doi: 10.1016/j.ijrobp.2014.07.048.
- 198 Allison RR, Bagnato VS, Sibata CH (2010) Future of oncologic photodynamic therapy. *Future Oncol* 6(6):929–  
199 940
- 200 Azizian G, Riyahi-Alam N, Haghgoo S, Moghimi HR, Zohdiaghdam R, Rafiei B, Gorji E (2012) Synthesis route  
201 and three different core-shell impacts on magnetic characterization of gadolinium oxide-based nanoparticles as  
202 new contrast agents for molecular magnetic resonance imaging. *Nanoscale Res Lett* 7(1):549
- 203 Babaei M, Ganjalikhani M (2014) The potential effectiveness of nanoparticles as radio sensitizers for  
204 radiotherapy. *Bioimpacts* 4(1):15.
- 205 Bernard BK, Osheroff MR, Hofmann A, Mennear JH (1990) Toxicology and carcinogenesis studies of dietary  
206 titanium dioxide-coated mica in male and female Fischer 344 rats. *J Toxicol Environ Health* 29(4):417–429
- 207 Bischoff F, Bryson G (1982) Tissue reaction to and fate of par- enterally administered titanium dioxide. I. The  
208 intraperitoneal site in male Marsh-Buffalo mice. *Res Commun Chem Pathol Pharmacol* 38(2):279–290
- 209 Bump EA, Hoffman SJ, Foye WO, Abraham DJ (2003) Radiosensitizers and radioprotective agents. In:  
210 Abraham DJ (ed) *Chemotherapeutic drugs, Burger's medicinal chemistry and drug discovery*, Vol 5. John Wiley,  
211 New York, pp 151–211
- 212 Chatterjee DK, Fong LS, Zhang Y (2008) Nanoparticles in photodynamic therapy: an emerging paradigm. *Adv*  
213 *Drug Deliv Rev* 60(15):1627–1637
- 214 Fabian E, Landsiedel R, Ma-Hock L, Wiench K, Wohlleben W, van Ravenzwaay B (2008) Tissue distribution  
215 and toxicity of intravenously administered titanium dioxide nanoparticles in rats. *Arch Toxicol* 82(3):151–157

216 Fang C, Zhang M (2009) Multifunctional magnetic nanoparticles for medical imaging applications. *J Mater*  
217 *Chem* 19(35):6258–6266

218 Garnica-Garza HM (2009) Contrast-enhanced radiotherapy: feasibility and characteristics of the physical  
219 absorbed dose distribution for deep-seated tumors. *Phys Med Biol* 54(18) 5411–5425

220 Hainfeld JF, Slatkin DN, Focella TM, Smilowitz HM (2006) Gold nanoparticles: a new X-ray contrast agent. *Br*  
221 *J Radiol* 79(939):248–253

222 Huo S, Ma H, Huang K, Liu J, Wei T, Jin S, Zhang J, He S, Liang XJ (2013) Superior penetration and retention  
223 behavior of 50 nm gold nanoparticles in tumors. *Cancer Res* 73(1):319–330

224 Jin C, Tang Y, Yang FG, Li XL, Xu S, Fan XY, Huang YY, Yang YJ (2011) Cellular toxicity of TiO<sub>2</sub>  
225 nanoparticles in anatase and rutile crystal phase. *Biol Trace Elem Res* 141(1-3):3–15

226 Kim BY, Rutka JT, Chan WC (2010) Nanomedicine. *N Engl J Med* 363(25):2434–2443

227 Kim D, Yu MK, Lee TS, Park JJ, Jeong YY, Jon S (2011) Amphiphilic polymer-coated hybrid nanoparticles as  
228 CT/MRI dual contrast agents. *Nanotechnology* 22(15):155101

229 Leon S, Zdenka K, Kostya O, Shailesh K (2012) Nanoparticles in cancer imaging and therapy. *J Nanomater*  
230 Vol(2012), Article ID 891318

231 Maeda H, Wu J, Sawa T, Matsumura Y, Hori K (2000) Tumor vascular permeability and the EPR effect in  
232 macromolecular therapeutics: a review. *J Control Release* 65(1-2):271–284

233 Nakayama M, Sasaki R, Ogino C, Tanaka T, Morita K, Umetsu M, Ohara S, Tan Z, Nishimura Y, Akasaka H,  
234 Sato K, Numako C, Takami S, Kondo A (2016) Titanium peroxide nanoparticles enhanced cytotoxic effects of  
235 X-ray irradiation against pancreatic cancer model through reactive oxygen species generation in vitro and in vivo.  
236 *Radiat Oncol* 11(1):91

237 Perrault SD, Walkey C, Jennings T, Fischer HC, Chan WC (2009) Mediating tumor targeting efficiency of  
238 nanoparticles through design. *Nano Lett* 9(5):1909–1915

239 Service RF (2005) Materials and biology: Nanotechnology takes aim at cancer. *Science* 310(5751):1132–1134.

240 Srivastava SK, Yamada R, Ogino C, Kondo A (2013) Biogenic synthesis and characterization of gold  
241 nanoparticles by Escherichia coli K12 and its heterogeneous catalysis in degradation of 4-nitrophenol. *Nanoscale*  
242 *Res Lett* 8(1):70

243 Townley HE, Kim J, Dobson PJ (2012) In vivo demonstration of enhanced radiotherapy using rare earth doped  
244 titania nanoparticles. *Nanoscale* 4(16):5043–5050

245 Ruba T, Tamilselvi R (2018) Radiosensitizers and radioprotectors for effective radiation therapy—A review.  
246 *Asian J Appl Sci Eng* 2(1):77–86

247 Wilson BC, Patterson MS (2008) The physics, biophysics, and technology of photodynamic therapy. *Phy Med*  
248 *Biol* 53(9):R61–R109

249 Yamaguchi S, Kobayashi H, Narita T, Kanehira K, Sonezaki S, Kubota Y, Terasaka S, Iwasaki Y (2010) Novel  
250 photodynamic therapy using water-dispersed TiO<sub>2</sub> polyethylene glycol compound: evaluation of antitumor effect  
251 on glioma cells and spheroids in vitro. *Photochem Photobiol* 86(4):964–971

252 Yezhelyev MV, Gao X, Xing Y, Al-Hajj A, Nie S, O'Regan RM (2006) Emerging use of nanoparticles in  
253 diagnosis and treatment of breast cancer. *Lancet Oncol* 7(8):657–667

254 Yin JJ, Liu J, Ehrenshaft M, Roberts JE, Fu PP, Mason RP, Zhao B (2012) Phototoxicity of nano titanium  
255 dioxides in HaCaT keratinocytes—generation of reactive oxygen species and cell damage. *Toxicol Appl*  
256 *Pharmacol* 263(1):81–88

257

258

259

## 260 **Figure Legends**

261 **Fig. 1** Characteristics of titanium dioxide nanoparticles (TiO<sub>2</sub>-NPs) (a) Representative transmission electron  
262 microscopy image of the TiO<sub>2</sub>-NPs. Their diameter is approximately 50 nm. (b) Size distribution of the TiO<sub>2</sub>-  
263 NPs as measured using dynamic light scattering.

264

265 **Fig. 2** Magnetization hysteresis loop of the titanium dioxide nanoparticles (TiO<sub>2</sub>-NPs)

266

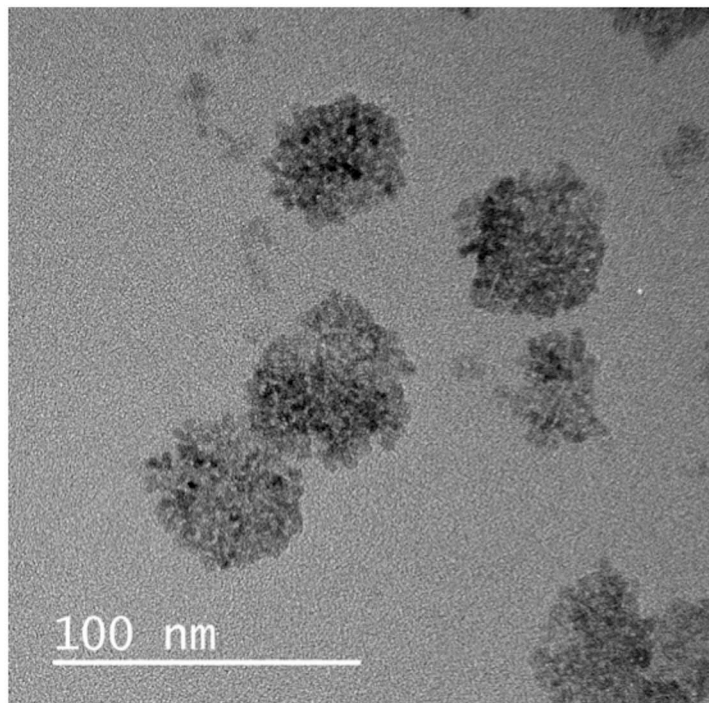
267 **Fig. 3** Colony forming assay results after exposure of MIAPaCa-2 to graded dose of X-ray radiation combined  
268 with TiO<sub>2</sub>-NPs. \*P<0.05 and \*\*P<0.1.

269

270 **Fig. 4** (a, b) Computed tomographic images and the corresponding Hounsfield unit values of the titanium  
271 dioxide nanoparticles (TiO<sub>2</sub>-NPs) (c, d) T<sub>1</sub>-weighted magnetic resonance images and the corresponding T<sub>1</sub>  
272 relaxation rates (1/T<sub>1</sub>) (e, f) T<sub>2</sub>-weighted magnetic resonance images and the corresponding T<sub>2</sub> relaxation rates  
273 (1/T<sub>2</sub>)

274

a)



b)

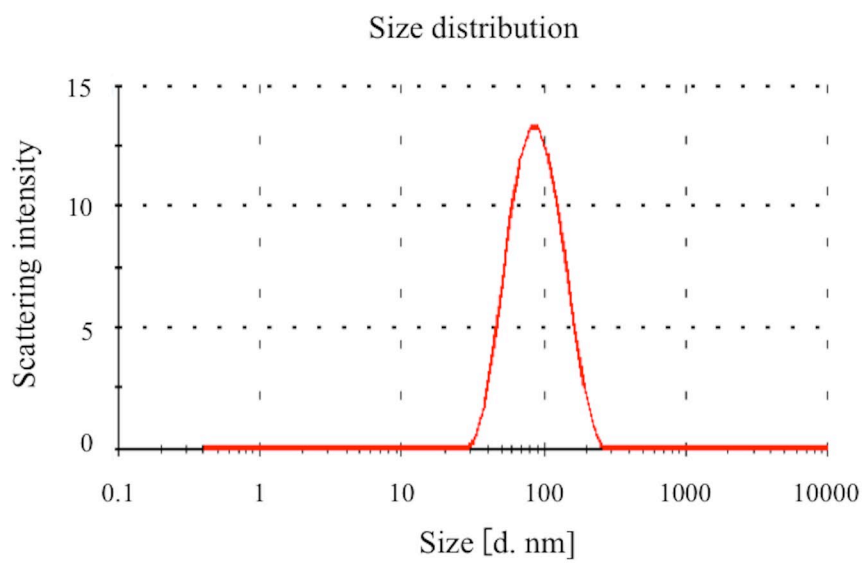


Fig.1 Akasaka et al.

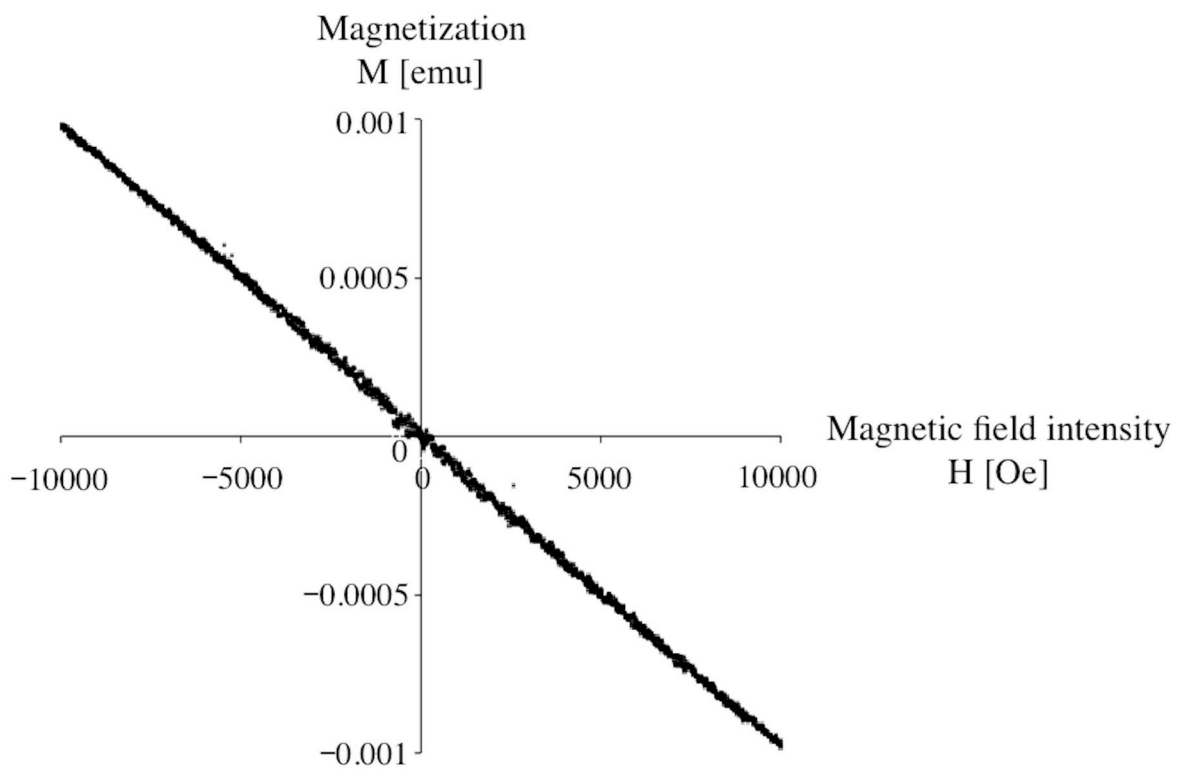


Fig.2 Akasaka et al.

# MIAPaCa-2

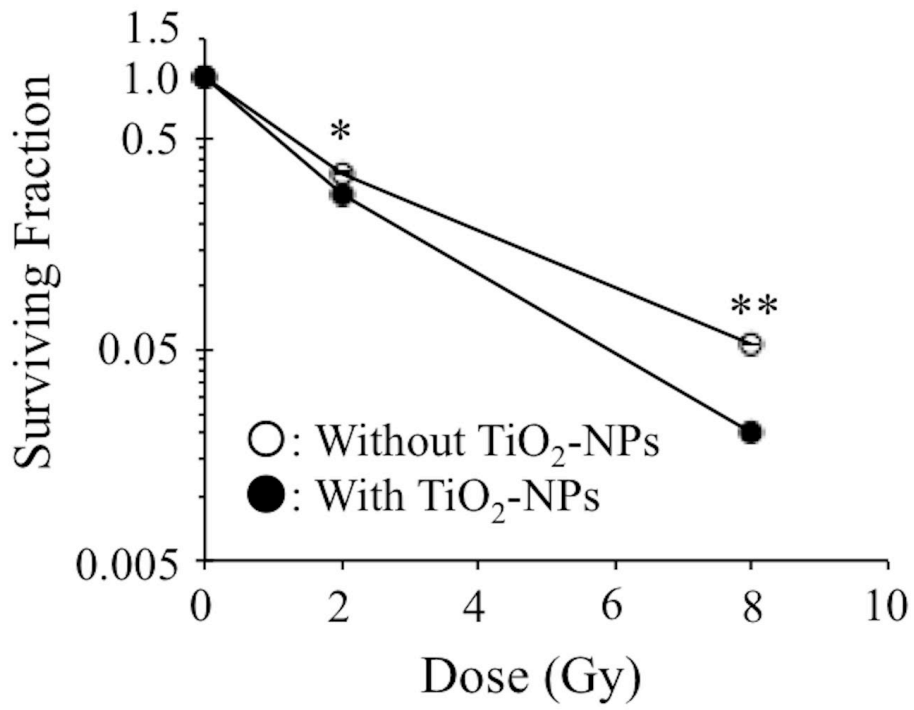


Fig.3 Akasaka et al.



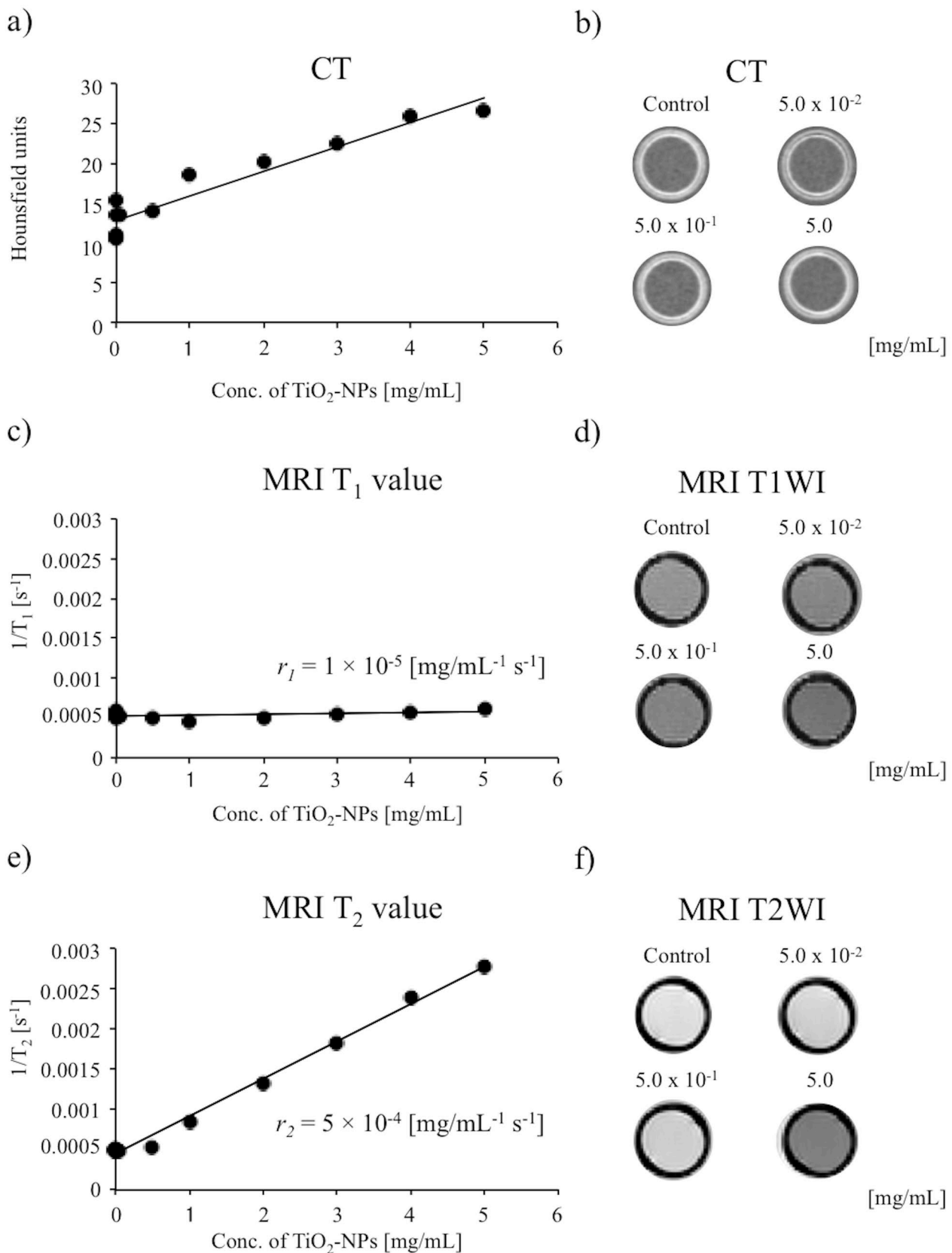


Fig.4 Akasaka et al.

Table 1. The CT values, T<sub>1</sub> values, and T<sub>2</sub> values of TiO<sub>2</sub>-NPs at each concentrations.

Concentration of TiO <sub>2</sub> -NPs [mg/mL]	CT value [HU]	T <sub>1</sub> value [msec]	T <sub>2</sub> value [msec]
0.0	13.4	1970.1	2046.8
$5.0 \times 10^{-6}$	10.5	1811.5	2014.8
$5.0 \times 10^{-5}$	10.8	1728.2	1974.8
$5.0 \times 10^{-4}$	11.0	1715.6	1999.4
$5.0 \times 10^{-3}$	15.3	1939.9	2046.8
$5.0 \times 10^{-2}$	13.4	1905.3	2047.0
$5.0 \times 10^{-1}$	13.9	2020.9	1895.4
1.0	18.5	2202.5	1191.2
2.0	20.1	1968.2	754.3
3.0	22.4	1810.9	548.1
4.0	25.8	1770.0	417.1
5.0	26.5	1614.4	360.8